JOURNAL OF SOLID STATE CHEMISTRY 7, 109–123 (1973)

Electrical Transport Properties and Preparation of the Metal–Ammonia Compound Lithium Tetraammine*

M. D. ROSENTHAL AND B. W. MAXFIELD†

Laboratory of Atomic and Solid State Physics, Cornell University, Ithaca, New York 14850

Received August 4, 1972

On specimens of the compound lithium tetraammine, $Li(NH_3)_4$, the resistance from 10 to 100°K and the magnetoresistance at 4.2 and 1.66 K have been measured. Measurements were made using a probeless, mutual inductance technique. Specimen preparation and aspects of the measurement technique used in preparing well mixed, homogeneous specimens are described. The resistivity shows several anomalies in the solid phase, one of which has also been observed in thermal measurements and is associated with a transition from an fcc to an hcp structure. The second, near 69 K, has not been observed in thermal measurements. It is suggested that this anomaly is characteristic of the compound $Li(NH_3)_4$ and may be a Martensitic or magnetic transition. The magnetoresistance is large with a marked decrease in slope above 50 kG. These results are compared with standard galvanomagnetic theory for compensated and uncompensated metals. In conjunction with arguments based on a free electron construction of the Fermi surface, it is concluded that lithium tetraammine is probably an uncompensated metal with a high proportion of carriers in open orbits.

I. Introduction

The systems formed by the dissolution in liquid ammonia of alkali and other metals, such as europium, calcium, strontium and barium, have provided an intriguing focus for the study of a host of chemical and physical phenomena. In the past decade there have been numerous studies of the thermodynamic and transport properties of the liquid solutions, with particular emphasis on the metal–non-metal transition which is observed as the concentration of the metal solute is increased (*1–4*).

Metal–ammonia compounds and in particular lithium tetraammine have received much less attention than the dilute and concentrated solutions. Little is known of the physical or electronic structure of lithium tetraammine; the phase diagram near the freezing point has not been well established and measurements on the solid have not been extensive. The present resistance and magnetoresistance study was begun when the literature was even more scant than that which exists currently. Considerable care has been taken to prepare specimens of known stoichiometry and to develop reproducible specimen handling and preparation techniques.

The earliest work was done by Jaffe (*5*), who in 1935 measured the melting point of the solid (20 mole% metal) as well as the Hall coefficient and the magnetoresistance at 77 K. Mammano and Coulter (*6*) measured the high-temperature specific heat from 60 K to the melting point, near 90 K, and Morgan and Thompson (*7*) measured the lattice specific heat from 2.2 to 4.2 K. Cate and Thompson (*8*) observed that below 4.2 K the resistivity was dominated by a quadratic term. In the temperature region above 60 K, resistivity measurements of Morgan *et al.* (*9*) indicated two solid–solid phase transitions, one near 69 K and one at 82 K. The specific heat measurements of Mammano and Coulter (*6*) confirmed the phase transition at 82 K, but they found no evidence for the 69 K transition in their thermal measurements. Later resistivity studies by McDonald and Thompson (*10*) also indicate that phase transitions exist near 69 K and 82 K. Their magnetoresistance measurements at 4.2 K show a quadratic field dependence,

* This work was supported by the Advanced Research Projects Agency through the Materials Science Center of Cornell University, Report #1807.

† Alfred P. Sloan Research Fellow

although later work by Lemaster and Thompson (*11*) indicates a smaller field dependence.

The structure of lithium tetraamine is also not determined completely. X-ray measurements were made at 77 K by Mammano and Sienko (*12*) who indicated that the transition near 82 K may be a Martensitic phase transformation with a high-temperature fcc phase and a low-temperature hcp phase. No X-ray data exist at other temperatures, so the nature of a 69 K phase transition is not established. In fact, it is not definitely related to the compound $Li(NH_3)_4$. In addition, there is conflicting data (*6*, *9*) for the exact stoichiometry of the compound at 88 K, if it is in fact a compound. Different experiments indicate either 4.0:1 or 4.15:1 for the ratio of ammonia to lithium.

II. Theory

The topology of the Fermi surface plays an important role in determining both the resistance and magnetoresistance of a metal (*13*). The simplest construction of the Fermi surface is made by calculating the radius of the free electron sphere, k_F, from the expression

$$k_F^3 = 3Z\Omega/8\pi,$$

where Z is the number of valence electrons per unit cell and Ω is the volume of the Brillouin zone (BZ) in momentum space. It is the size of the free electron sphere compared to the BZ that is important in determining the various transport properties in a magnetic field. If the free electron sphere lies well within the first BZ, then the actual Fermi surface will be distorted from the ideal spherical geometry but it is not likely to make contact with the zone boundary. Under this condition which, for instance, is the case for the alkali metals, only closed electron orbits are possible. When the free electron sphere comes close to the zone boundary, as it does in the well-known case of copper, the actual Fermi surface will be distorted such that at some regions, it contacts the zone boundary. This gives rise to extended orbits in momentum space as well as the possibility of both electron and hole orbits.

In interpreting magnetoresistance measurements, one important parameter is the ratio of the density of holes, n_h, to the density of electrons, n_e. If $n_h = n_e$ the metal is said to be compensated; otherwise it is uncompensated. The state of compensation, being determined by the net number of carriers per unit cell, n_a, is given by (*13*)

$$n_a = 2(F+J) - sZ, \tag{1}$$

where F is the number of full zones, J is the number of zones containing holes, Z is the valence and s is the number of atoms per unit cell. If sZ is odd, n_a can never be zero and the metal cannot be compensated. If sZ is even, the metal may be either compensated ($n_a = 0$) or uncompensated ($n_a \neq 0$). All metals with even sZ are known experimentally to be compensated. However, if $2J \neq sZ - 2F$, the metal will not be compensated. This should be the case for monovalent, hexagonal close packed (hcp) metals with small spin-orbit coupling; here there are not only no full zones (i.e., $F = 0$) but no zones having hole orbits (i.e., $J = 0$). With small spin-orbit coupling, the fundamental zone becomes a double zone (*14*).

Figure 1 shows the free electron constructions for both single and double zones for a monovalent hcp metal with c/a ratio $\geqslant 1.43$. When the free electron sphere intersects a BZ boundary, it is possible, following the procedure of Harrison (*15*), to remap those zones which are filled or

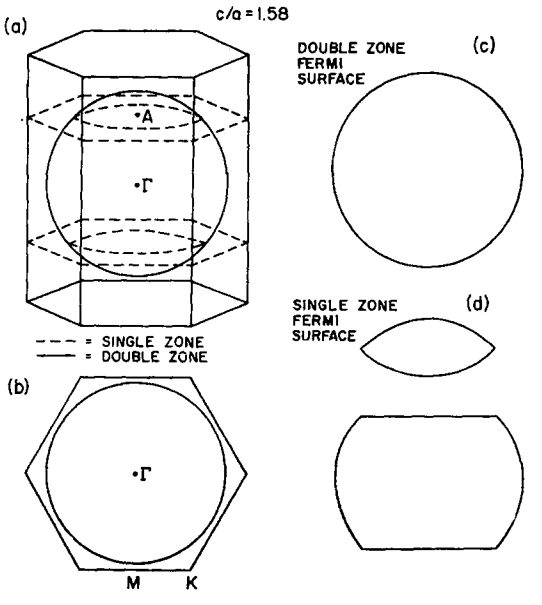

FIG. 1. Free electron construction of the Fermi surface of lithium tetraammine: (a) perspective showing single and double zones with free electron sphere inscribed. (b) Cut perpendicular to c-axis showing approach of free electron sphere to zone boundaries, (c) double zone Fermi surface, (d) single zone Fermi surface.

partially filled into the first BZ. This can always be done since the volumes of all zones are equal. Except in magnetic materials the Fermi surface so constructed bears a remarkable resemblance to the actual Fermi surface.

The interpretation of magnetoresistance observations is best done by using the basic approach of Lifschitz, Azbel' and Kaganov (LAK) (*16*). As long as the scattering processes are independent of the magnetic field, the high-field magnetoresistance is determined completely by the electronic band structure. The magnitude of the magnetoresistance is normally described in terms of the zero-field resistivity. If $\rho(H)$ is the resistivity in a field H, then $[\rho(H) - \rho(0)]/\rho(0) = \Delta\rho/\rho(0)$ is the magnitude of the magnetoresistance; a large magnetoresistance implies that $\Delta\rho \gg \rho(0)$.

Many of the gross features of the magnetoresistance depend upon whether or not the metal is compensated. In the high-field limit, a compensated metal is predicted to have a large, quadratic magnetoresistance (*16*, *13*). In practice all single crystal, compensated metals exhibit such behavior in the high-field limit. However, the high-field behavior of many polycrystalline, compensated metals is more closely represented by a 1.8 or 1.9 power law (*17*).

In an uncompensated, single crystal metal the magnetic field behavior is determined by the orbit structure in the plane normal to the magnetic field. With only closed orbits, the high-field magnetoresistance saturates, that is, becomes independent of magnetic field and is normally quite small, say $\Delta\rho \lesssim 10\rho(0)$ (*13*, *17*). If there are open orbits in the plane normal to the magnetic field, then the magnetoresistance is predicted to have a quadratic component; the larger the number of open orbit carriers, the larger the quadratic component (*13*). It is difficult to predict the exact field dependence that would be observed in a polycrystalline specimen when there exist both open and closed orbits. However, in the high-field limit, most polycrystalline, uncompensated metals have a modest magnetoresistance [$\Delta\rho < 100\rho(0)$ in a 100 kG field] that can be characterized approximately by a 1.3–1.5 power law (*17*).

III. Experimental Techniques

A. Specimen Preparation

Lithium tetraammine specimens were prepared by condensing ammonia gas into pyrex tubes which contained previously cleaned and weighed quantities of 99.9% purity Li (*18*). The following sections describe the preparation of the specimen tubes, the cleaning of the ammonia (including a description of the vacuum line used for metering and distillation of the ammonia) and the cleaning of the lithium.

i. Preparation of the Sample Tubes. Evidence gathered over more than a two-year period showed that lithium tetraammine specimens could be stored in liquid nitrogen for essentially indefinite periods of time with no measurable signs of deterioration. However, the specimen temperature must rise above 77 K during preparation (to ensure uniform mixing and complete dissolution), mounting and unmounting of the specimen. Many measurements were also performed above 77 K. Because it is known that impurities either in the specimen or adsorbed to the glass wall tend to promote decomposition at elevated temperatures (*19*, *20*), every precaution was taken to ensure cleanliness.

A schematic representation of the specimen preparation procedure is shown in Fig. 2. Standard pyrex tubing sealed at one end and connected to a ground glass joint at the other was used for the specimen tubes. The chemistry of the glass–metal–ammonia interface is not well understood. A number of cleaning procedures have been described in the literature (*9*, *19–21*). The major goal is to remove from the glass wall as much of the adsorbed water as possible, since this may promote the decomposition of the metal–ammonia solution (*22*).

The success of our procedure is indicated by the stability of the solutions for long periods of time, both at 77 K and 200 K. A sealed specimen, made to test the stability of the concentrated solution, was allowed to warm to room temperature. This specimen showed only slight visual degradation after 24 hr and after about two weeks the specimen tube exploded, probably due to the formation of lithium amide and the release of hydrogen gas. A three-step specimen tube cleaning procedure was followed. The pyrex tubes described above were first washed with a solution of nitric acid, hydrofluoric acid, and water. This process presumably replaces adsorbed water with the fluorine ions (*19*). After filling with the acid solution, the tubes were allowed to stand for ten or fifteen min; they were then rinsed with distilled water a minimum of fifteen times in order to remove all traces of the acid and placed in a small vacuum

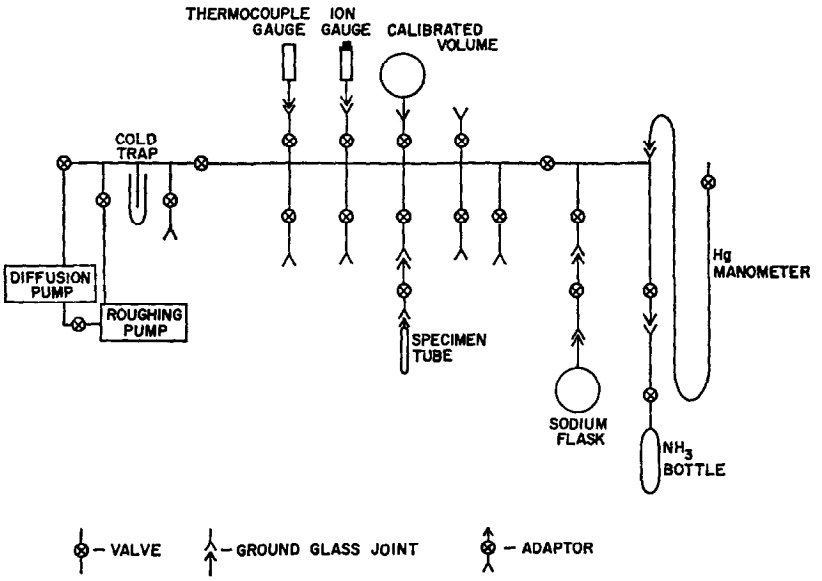

FIG. 2. Vacuum line for preparation of clean ammonia showing Hg manometer and calibrated volume used to allow measured amounts of ammonia to be condensed into specimen tubes.

oven (about 100 Torr). After baking at 100°C for a few hours, they were connected to the vacuum line with stopcock adapters (see Fig. 2). When the pressure dropped to below 10^{-4} Torr, the tubes were heated until they glowed orange. The first flaming produced a noticeable increase in the line pressure. Upon cooling, the pressure would drop to between 10^{-5} and 10^{-6} Torr. The flaming procedure was repeated until there was no longer any increase in pressure upon further heating. This completed the second step in the cleaning procedure.

Next, about 500 Torr of ammonia was introduced into the vacuum line, allowed to sit for approximately one-half hour, and then cryopumped into a cold trap with liquid nitrogen to a pressure below 5×10^{-3} Torr. After closing the stopcocks, the adapters were removed from the vacuum line and introduced into a helium filled glove box in which the lithium was prepared. Inside the glove box, the tubes were removed from the adapters. Therefore, after cleaning, the tubes were not in contact with any atmosphere except the inert helium gas used in the dry box.

ii. Ammonia Preparation. The second important aspect of the specimen preparation was the production of pure, anhydrous ammonia. Ammonia of 99.99% stated purity was used as a starting material (*23*). The simple test of measuring the residual pressure of an ammonia sample condensed into a cold trap at 77 K showed that the noncondensable vapors were within this specification. The ammonia was purified further as follows. A 100-cc flask containing pieces of sodium metal (loaded in the glove box in the manner described in the next section for the lithium) was placed on the vacuum line. Ammonia was then condensed into the flask using liquid nitrogen; the residue was pumped off using a diffusion pump. After closing the stopcock connecting the flask to the vacuum line, the liquid nitrogen was replaced with a dry ice–alcohol bath. The sodium was of a quantity to ensure a saturated solution of sodium in ammonia; as the flask warmed, the metal dissolved in the liquid ammonia. The dissolved sodium will react with any residual water and oxygen that may be in the ammonia (these materials are not removed by fractionation at 77 K). All specimens were prepared from ammonia which had been left on the vacuum line in contact with excess sodium for periods of a week or more.

In order to determine the quality of the ammonia that was prepared in this manner, several specimens of ammonia were prepared in NMR tubes treated in the same manner as the resistivity specimen tubes described in the previous section. The room-temperature NMR spectrum was recorded using a Varian A60 NMR spectrometer. The types of spectra that were observed are shown in Fig. 3. Figure 3a is representative of several specimens; this is the characteristic

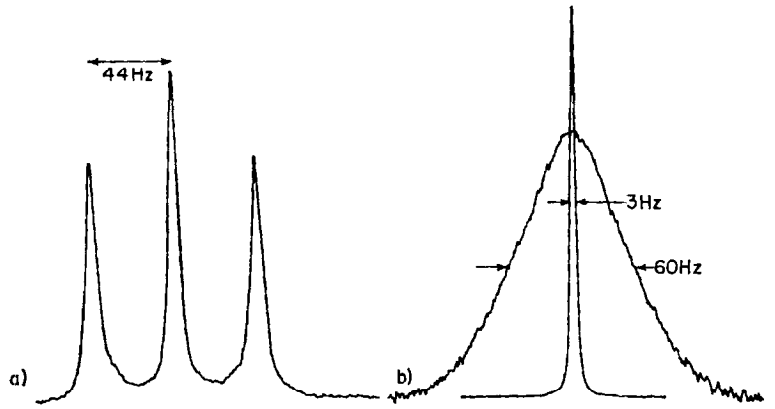

FIG. 3. Representative NMR spectra of prepared ammonia: (a) triplet of dry ammonia used for some specimens, (b) broad singlet of typical specimen ammonia. Also, narrow singlet of ammonia doped with a few ppm water. Note that the scales are very different and that the area under these curves is the same.

triplet structure described by Ogg (*24*) who claimed that it is indicative of ammonia having a purity of better than a few parts per million water. Other samples as represented by Fig. 3b showed very broad singlets with half-widths of about 60 Hz. Several NMR tests were also made on ammonia to which between 10 and 20 parts per million of water had been added. This was done by condensing it into the NMR tube from other tubes containing water vapor. Samples prepared in this manner or samples which had been prepared in tubes without flaming, all showed a very narrow singlet with a half-width of about 3 Hz (also shown in Fig. 3b). The line broadening or the dramatic appearance of the triplet gives quantitative evidence that the ammonia used for specimen preparation always contained less than a few parts per million water, and that the specimen tube preparation essentially eliminated the residual water adsorbed to the glass walls.

For the preparation of lithium tetraammine specimens, the quantity of purified ammonia was determined by a volumetric technique. A nominal 1-liter flask, calibrated to about 0.1 % accuracy by filling with distilled water and measuring the change in weight, was attached to the vacuum line. To correct for deviations from ideal gas behavior, we chose the Beattie–Bridgeman equation utilizing the coefficients for ammonia listed in Castellan (*25*). For large specimens and the highest ammonia pressures that were used, the deviations from ideal gas behavior were roughly 10%. (The pressure was always kept below one atmosphere in order to ensure positive sealing of the ground glass joints and valves on the vacuum line. Specimens requiring greater amounts of ammonia were prepared with more than one distillation.)

The accuracy of this correction was tested by calculating the density of ammonia at STP. Our calculated value of 0.7705 g/liter compares well with an accepted value (*26*) of 0.7712 g/liter. During the preparation procedure, it was necessary to continuously monitor the room temperature. The desired pressure of ammonia was calculated using an interactive APL computer terminal. The pressure was measured using a mercury manometer attached to the vacuum system. Each mercury miniscus was covered with a small quantity of diffusion pump oil (*27*) to prevent distillation of mercury vapor into the specimens. The manometer could be read to slightly better than 1 mm. Since typical large samples required over 500 mm of ammonia, the error introduced by the pressure measurements was about 0.2%. Corrections, amounting to about 0.4 %, were made for the thermal expansion of the mercury in the manometer.

After the ammonia had been driven from the sodium–ammonia mixture by warming, and nearly the desired pressure had been achieved, the stopcock on the flask was closed. When the pressure stabilized, indicating thermal equilibrium had been achieved, ammonia was added or subtracted as necessary. The stopcock on the calibrated volume was then closed and the remaining ammonia was condensed back into the distillation flask using liquid nitrogen. The line was cleared with the diffusion pump, and the ammonia in the calibrated volume was condensed into the specimen tubes (which at

this stage contained lithium prepared as outlined below) using liquid nitrogen. To guarantee that all the ammonia in the calibrated volume had condensed into the specimen tubes, the pressure was monitored using a thermocouple gauge. Specimen tubes were closed to the line only after the pressure was below 50 μm. Since the total volume of the line was only 50% greater than the calibrated volume, the residual ammonia left in the line was negligible. The total error involved in determining the amount of ammonia in the larger specimens, that is, those requiring more than 50 mm of ammonia, was about 0.3%.

iii. Preparation of the Lithium. A helium atmosphere was chosen for the glove box since at room temperature lithium metal reacts with both nitrogen and oxygen. A pure helium atmosphere was obtained by purging with a helium gas bag within the glove box and backfilling with helium gas forced from a liquid helium storage vessel. The box was then flushed with helium; the excess gas being removed continuously by pumping. The quality of the atmosphere was noted by observing the surface contamination of a pool of molten sodium. When no surface film was observable for $\frac{1}{2}$ hr or more, the flushing was stopped.

In order to reduce the remaining contaminants to a minimum, the helium atmosphere was continually recirculated through a drying train consisting of a liquid nitrogen precooler and a liquid nitrogen cooled, activated-charcoal trap. These were effective in removing all contaminants except for the inert gases with low boiling points. As far as could be determined, the remaining contaminants produced no undesirable effects. After two or three weeks of continuous operation, the quality of the atmosphere was extremely good. A piece of potassium with freshly cut surfaces would show only very slight visible contamination after 24 hr, and a quantitative test showed that a 30-mg square piece of potassium with freshly cut surfaces changed weight by less than 5 μg in 24 hr. To ensure cleanliness and to remove the traces of contaminants introduced by putting the sample tubes into the box, the glove box was always flushed with dry helium for at least 1 hr before the lithium pieces were prepared.

The lithium (*18*), supplied in $\frac{1}{2}$-in. diameter rods under oil, was first washed in xylene to remove the oil. The xylene was removed by pumping in the vacuum port prior to placing the lithium in the glove box. Pieces of lithium were prepared by slicing a thin disc from the rod and cutting away the exterior surface layers. Cutting was done using either a stainless steel razor blade held in a hemostat, or a commercial blade and holder combination. To ensure cleanliness, the blades were degreased by washing in soap and water and then rinsing in acetone, distilled water and finally with absolute alcohol. The blades were baked in a vacuum oven to guarantee that the surfaces were free of water and other volatile residues. Generally, the pieces of lithium cut from the interior of the rod were bright and shiny. Occasional surface discoloration was noticed if the lithium happened to adhere to the cutting blade. It is surmised that in this situation the coldworking necessary to cut and then remove the piece from the blade raised the temperature of the lithium sufficiently for it to react with residual contaminants in the glove box. Blades were generally used only once or twice, since the probablity of sticking was greatly increased with further use. The resulting discs, which were free of oxide or nitride contamination were cut into smaller pieces which could be inserted through the 10/30 ground glass joint on the vacuum line adapters. The largest such piece was about 25 mg, hence several pieces of lithium were needed for most specimens. While this made the preparation task more difficult, it meant that the dissolution of the lithium in the ammonia occurred more readily. The lithium pieces were weighed inside the glove box using a Cahn electrobalance having a sensitivity of 0.1 μg and a linearity of 0.01%; the electrical connections were made via vacuum feedthroughs. The balance was calibrated using a 50 mg calibration weight (*28*). A digital voltmeter having 0.01% linearity and 1 μV resolution was used for the balance readout. Zero drifts and other noise due to vibrations of the glove box produced a total maximum error of about 0.1% in determining the weight of lithium used for any specimen.

The weighed lithium was inserted into the specimen tubes, evacuated to 100 μm, removed from the glove box, placed on the vacuum line and evacuated to approximately 10^{-6} Torr. Then a measured amount of ammonia was condensed into the specimen tubes and they were sealed permanently by melting. To complete mixing after sealing, the specimens were placed in a dry ice–alcohol bath for about 15 min. Inhomogeneities in the specimen could be detected by examining the frequency dependent mutual resistance, ΔR, described in Section IIIB. Deviations from a slope of 2 in a plot of ΔR vs frequency indicate that the solid is not homo-

geneous. When specimens displayed this behavior, further mixing in the dry ice bath produced a slope of 2. All resistivity data presented later are for specimens prepared with 4:1, NH_3:Li, mole ratios.

B. Resistivity Measurements

Because of the difficult experimental problems involved in determining the resistivity of lithium tetraammine using standard four-terminal techniques, we chose to use a probeless, constant excitation, ac method. This offers the possibility of convenient, continuous data readout, a feature not available using the eddy-current decay method. Phase-sensitive detection can also be used to improve the sensitivity.

The method used is described in more detail elsewhere (*29*), but in principle it is the same as that described by Zimmerman (*30*). The metallic specimen is placed in the center of a coaxial mutual inductor; the primary coil is driven with a sinusoidal current, and the mutual impedance between the two coils is measured. The presence of eddy currents in the specimen changes both the mutual inductance and mutual resistance compared to the same measurement performed when the specimen is removed. In general, power losses in the specimen cause an increase in the mutual resistance and the surface screening currents reduce the mutual inductance. It can be shown, for infinite cylindrical geometry, that if the mutual resistance in the absence of the specimen is small compared to the mutual resistance with the specimen inserted, then the changes in mutual resistance and mutual inductances are given by

$$\Delta R = \gamma(\mu/\mu_0)\omega L_0 f_i(\alpha) \tag{2}$$

$$\Delta M = -\gamma L_0[(\mu/\mu_0)f_r(\alpha) - 1] \tag{3}$$

where $\omega/2\pi = \nu$ is the frequency of the excitation current, L_0 is the self inductance of the empty coils (the primary and secondary coils are assumed to be identical and perfectly coupled), μ is the magnetic permeability of the specimen, γ is a filling factor equal to the ratio of the specimen to coil cross-sectional area, $\alpha = \omega\sigma\mu a^2$, σ is the dc conductivity, a is the specimen radius and f_i and f_r are the imaginary and real parts, respectively, of the function

$$f(\alpha) = \frac{2I_1(i^{1/2}\alpha)}{i^{1/2}\alpha I_0(i^{1/2}\alpha)}.$$

$I_n(x)$ is the modified Bessel function of order n. Figure 4 shows ΔR and ΔM given by Eqs. (2) and (3), respectively. Although these expressions are only exact for an infinite cylindrical geometry, Fig. 4 shows that within the experimental accuracy of about 1%, Eq. (2) also predicts the mutual resistance of a copper calibration specimen. In the low-frequency limit, that is, when the skin

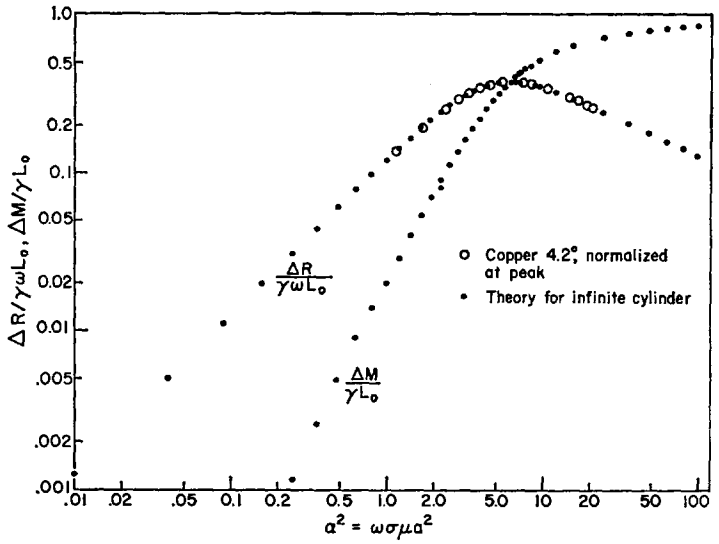

FIG. 4. Calculated results for the resistive and inductive changes, ΔR and ΔM; plotted vs the dimensionless parameter $\alpha^2 = \omega\sigma\mu a^2$ for an infinite right circular cylinder of conductivity, σ, placed in an infinite, coaxial mutual inductor. For comparison, the resistive change for a copper cylinder is also shown. The data is normalized to the theoretical results by matching the valve at the peaks of the curves.

depth, $\delta = (2/\mu_0\sigma\omega)^{1/2}$, is much larger than the specimen radius, Eq. (2) simplifies to give

$$\Delta R = \tfrac{1}{8}\gamma\omega L_0(\omega\sigma\mu a^2). \quad (4)$$

As described in Section IIIA, the quadratic frequency dependence, derived assuming a homogeneous metal, was used during specimen preparation to determine when they had been mixed properly. The frequency dependence of the mutual resistance shown in Fig. 4 was also used to determine the presence of significant inhomogeneities in the resistivity of several specimens at low temperatures. The squares in Fig. 5 show results of a frequency scan, $\Delta R/\nu$ as a function of frequency, for a lithium tetraammine specimen allowed to anneal for a period of 24 hr or more at temperatures slightly below the liquid–solid and solid–solid phase transitions and then cooled slowly to 4.2 K. The solid curve in the vicinity of these points is the theoretical curve, Eq. (2). The distinct deviation of the data points from ideal behavior could result from a radial variation in the resistivity. For profiles in which the resistivity increases towards the surface, the effective specimen radius is less than the physical radius; this moves the peak in the curve to a higher frequency and makes the frequency dependence more broad. For specimens with a lower resistivity near the surface, the peak shift is to a lower frequency and the frequency dependence is narrowed.

As shown by the circles in Fig. 5, the frequency dependence is much different for a quenched specimen. After warming the specimen approximately 40 K above the melting point, it was plunged into a liquid helium bath and cooled to 4.2 K. This rapid cooling presumably preserves the homogeneity present in the liquid phase. The nearly ideal behavior after quenching leads us to believe that a nonuniform resistivity, perhaps due to impurity migration during either annealing or slow freezing, caused the nonideal behavior in the annealed specimens. All resistivity and magnetoresistivity measurements below 4.2 K were made on quenched specimens. The high-temperature results are essentially independent of the annealing state of the specimen. These results show some of the advantages of probeless methods in determining both the resistivity and other specimen properties.

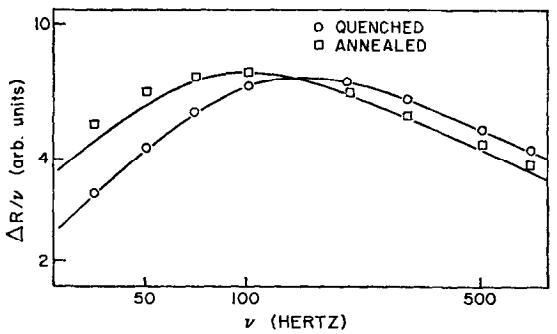

FIG. 5. Frequency scan at 4.2 K, $\Delta R/\nu$ vs ν, for the same lithium tetraammine specimen; first for annealing below each transition and cooling slowly to 4.2 K and next when warmed 40 K above the melting point and quenched rapidly to 4.2 K. The solid lines are the theory for infinite cylinders normalized at the peak.

C. Other Experimental Aspects

Measurements of the resistivity of lithium tetraammine were made in the temperature range 1.5–100 K using the specimen holder and cryostat shown in Figs. (6) and (7). From 1.5 to 35 K, the temperature was measured using a calibrated germanium resistance thermometer. Above 35 K,

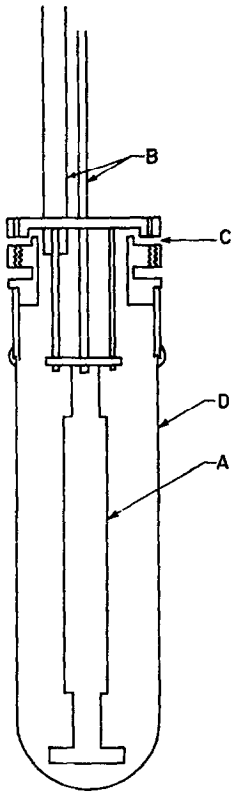

FIG. 6. Schematic drawing of cryostat and specimen holder: (A) Specimen holder. (B) Pumping lines. (C) Metal O-ring vacuum seal. (D) Glass vacuum chamber with glass-copper housekeeper seal.

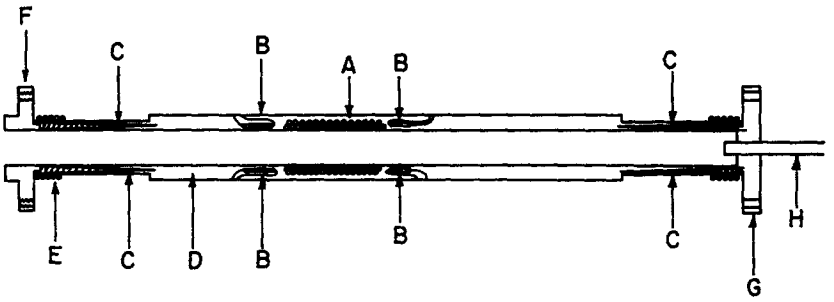

FIG. 7. Detail of specimen holder: (A) Mutual inductor. (B) Carbon resistance thermometers. (C) Feathered copper metal-plastic seals. (D) Epibond 100A specimen holder. (E) Heater coil. (F) Metal O-ring flange. (G) Brass flange. (H) Vacuum line.

the temperature was measured using a pair of gold-cobalt vs copper thermocouples. The thermocouples were calibrated using the known temperatures of ice, dry ice–alcohol, liquid nitrogen and liquid helium. Above 45 K, the accuracy of the temperature measurements is 0.1 K; from 10 K to 45 K, 0.2 K; and below 10 K, the accuracy improves steadily to about 0.1% at 4.2 K and below.

From 77 K down to 45 K, the temperature was changed by pumping on a liquid nitrogen bath. Thermal contact between the specimen and bath was achieved by introducing helium exchange gas into the outer chamber. Typical cooling and warming rates were about 2–3 K per hour or less. Slow temperature changes were desirable in order to maintain thermal equilibrium between the specimen (inside the plastic chamber, see Fig. 6), the thermocouples and germanium resistance thermometer (bonded to the specimen chamber with GE 7031 varnish), and the bath. Temperature gradients along the length of the specimen were minimized by comparing the thermocouple voltages at the top and bottom of the specimen holder and adjusting the power in the top and the bottom heater until the temperature difference was less than about 0.1 K. Radial temperature gradients were held to a minimum by slow cooling and warming rates. Temperatures below 45 K were obtained by transferring liquid helium on top of the small remaining amount of frozen nitrogen. While this is inefficient, the large thermal mass of the nitrogen caused the cryostat to cool and warm slowly. Above 77 K, the exchange gas chamber was evacuated and the specimen was warmed using the two heaters.

The quenching experiments already mentioned and the low-temperature resistance and magnetoresistance measurements to be described in the next section were made using a coil system similar to the one described in Section IIIB but without the elaborate exchange gas chambers and the temperature control. These were unnecessary since the specimen and holder were immersed directly in the liquid-helium bath and the temperature was controlled by regulating the vapor pressure of the helium with a Cartesian manostat. The temperature was measured with a calibrated germanium resistance thermometer and a four-terminal resistance bridge (*31*).

All magnetoresistance measurements were done in a 1.5 in. bore, 100 kG superconducting solenoid having an axial field homogeneity of better than 0.3% within ±1 in. of the magnet center. The entire specimen was within this homogeneous region. Field measurements accurate to 1% were made using a calibrated copper magnetoresistance probe. Resistivity measurements were made between 1 and 100 kG at 4.2 K and 1.66 K. The magnetoresistance data analysis is more complicated since there were reasonably large unavoidable resistive losses in both the dewar and magnet. Appropriate corrections for these losses were made as described elsewhere (*29*).

IV. Results and Discussion

A. High-Temperature Resistivity—10 K to 100 K

Figure 8 shows the temperature-dependent resistivity of lithium tetraammine from 10 to 100 K for a representative specimen. Above the melting point of 88.8 K, the resistivity is large, approximately 83 $\mu\Omega$-cm, with a negative temperature coefficient. Upon freezing, the resistivity drops by a factor of 6.1 and then continues to decrease slowly down to 82.2 K where there is

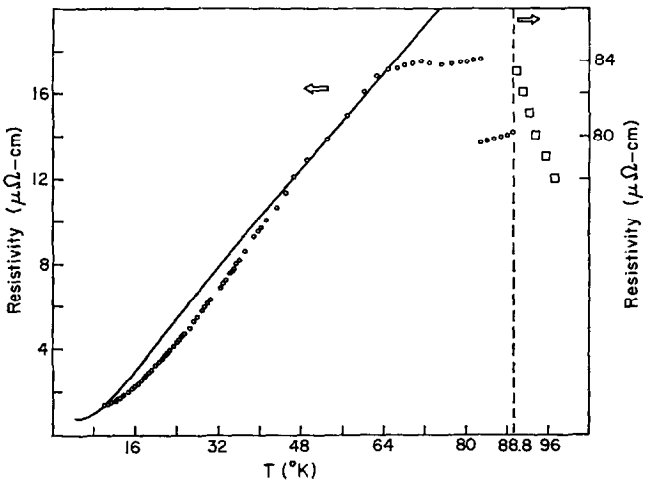

FIG. 8. Resistivity versus temperature of lithium tetraammine, 10–100 K. Solid line is the calculated Bloch-Gruneisen resistivity for $\theta_R = 54$ K and normalized at that temperature. The arrows indicate the proper scale to be used for results above and below the melting point, 88.8 K.

an increase of about 30%. Between 82.2 K and 68 K, the resistivity is almost constant. Below 64 K, it decreases rapidly.

The resistivity measurements shown in Fig. 8 were taken when the specimen was warming. The phase transitions exhibit considerable hysteresis; when cooling it is possible for them to be delayed to considerably lower temperatures. Figures 9 and 10 show typical curves taken when cooling the specimen through the transition points. As shown in Fig. 10, the minimum in the resistivity that occurs around 70 K also exhibits hysteresis.

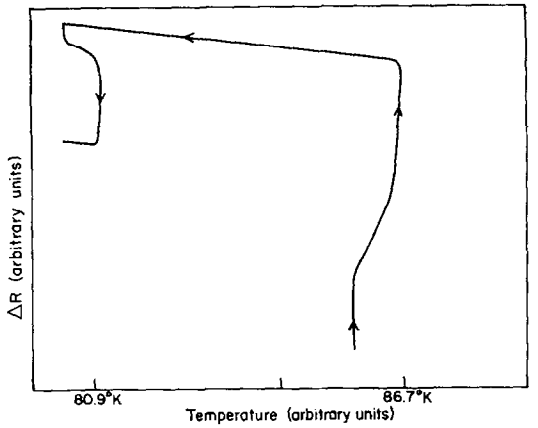

FIG. 9. Hysteresis of resistivity when cooling through the liquid–solid and solid–solid phase transitions near 89 K and 82 K, respectively; the specimen supercools through each transition and then warms as the transformation occurs. Although the temperature scale is arbitrary, the temperatures noted on the horizontal axis are exact and hence give a rough calibration.

The large drop in the resistivity upon formation of the solid can be explained qualitatively by using the suggestion of Mott (*32*) that the conductivity of any liquid metal and that of the solid are related by

$$\sigma_{sol}/\sigma_{liq} = \exp\{CL/T_m\},$$

where L is the latent heat, T_m the melting point and C is a constant. Using the data of Mammano and Coulter (*6*) for L, and the constant $C = 8.0 \times 10^{-2}$ K/J suggested in Meaden (*33*), the calculated ratio is 7.8. This suggests that any changes in the electronic structure and scattering mechanisms are not important in producing the change in resistance. Instead, the decreased resistivity of the solid is due to the increased order of the system. This is supported by measurements of the molar susceptibility, χ, which indicate that χ has the same value in both the solid and liquid states (*34*).

The sharp break in the resistivity near 82 K has been attributed to a change in crystal structure. Evidence for two crystal phases at 77 K is given by Mammano and Sienko (*12*), who indexed X-ray lines belonging to a fcc phase and an hcp phase with the intensity of the fcc lines becoming weaker with time. These lines indicate that the high-temperature phase persists to 77 K and that not all of the fcc phase transforms at 82 K. This behavior shows similarities to the Martensitic transformation in lithium and sodium where

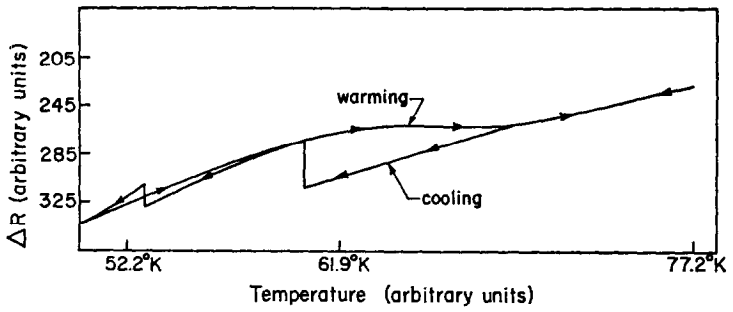

FIG. 10. Hysteresis of resistivity when warming and cooling from 52 K to 77 K. Note sharp breaks when cooling. Although the temperature scale is arbitrary, the temperatures noted on the horizontal axis are exact and hence give a rough calibration.

it has been estimated that at 4.2 K anywhere from 5 to 90% of the material has transformed (*35*).

In many respects, however the transformation is not at all like those found in lithium and sodium. First, the resistivity at 77 K for the tetraammine reaches a stable value after approximately 3 hr, and this value does not depend on the thermal history of the specimen. Contrary to the observations for lithium and sodium, this indicates that the percentage of material which transforms is always the same. Therefore, it is likely that the entire specimen has transformed. In addition, the reversion to the high-temperature phase occurs in a temperature range of less than 0.5 K compared to the order of 20 K for lithium and sodium. Secondly, the 30% decrease in resistivity (between the low-temperature hcp phase and the high-temperature fcc phase) is quite large. The corresponding increase in sodium is 10% while to within 0.8% there is no change in the resistivity of lithium. The observed large change in resistivity at 82 K could be due to several mechanisms that do not involve invoking drastic changes in the electronic structure [such as the assumption of complete compensation together with low carrier density (*10*)]. The Debye temperature, θ_D, of the two phases may differ considerably. For the hcp phase, specific heat measurements yield $\theta_D = 54$ K (*7*). Using the method discussed by Kelly and MacDonald (*36*), evaluation of the logarithmic derivative of the resistivity yields a value for θ_R, the resistance Debye temperature, of 150 K in the fcc phase. This would mean that upon cooling through the 82 K transition, the material transforms from a phase where $T < \theta_R$ to one where $T > \theta_R$ (since it is likely that $\theta_D \cong \theta_R$). The change in phonon scattering could then account for the increase in resistance.

However, it seems most likely that this increase is due to increased umklapp scattering. The change from fcc to hcp increases the number of electrons per unit cell from one to two. Therefore, in the hcp phase the Fermi surface is likely to be considerably closer to the zone boundaries. This makes umklapp scattering more likely. Umklapp scattering would be enhanced further in the low-temperature phase by a decrease in θ_D. It is not likely that dislocations or other crystal defects caused by the transformation could explain the large increase in resistivity. The defect contribution in lithium or sodium is relatively small as well.

The minimum in the resistivity near 70 K first reported by Morgan *et al.* (*9*) has not been explained. Thermal measurements of Mammano and Coulter (*6*) show no unusual characteristics in this temperature region. Figure 10 shows the hysteresis of a typical specimen between 77 and 52 K. On cooling, the resistivity exhibits as many as eight discontinuities which occur very rapidly. Typically two or three appear randomly between 52 and 72 K. From Fig. 10 it may be seen that the transitions occur without any detectable latent heat. (The discontinuities appear as vertical lines with no evidence of warming. Experiments show no detectable change in the cooling rate.) The large hysteresis, the fluctuation in position of the resistance minimum on heating, and the appearance on cooling of several jumps in the resistivity give this transition the appearance of a Martensitic phase transformation. However, the crystal structure below 77 K is not known.

Various explanations for these jumps in the resistivity are possible. They have been attributed to the transformation of fcc material which has supercooled (*11*). The specimen may also adhere to the glass walls and then contract suddenly.

The thermal anomaly seen in differential thermal analysis (DTA) measurements at these temperatures may be invoked (*37*). It is also possible that these jumps are due to the presence of excess lithium in the specimen.

These possibilities were tested in several ways. A specimen made with a 4.3:1 mole ratio of ammonia to lithium will have an ammonia concentration greater than that at which the DTA signal disappeared and the low-temperature solid should have no excess lithium. Measurements on such a specimen showed the same hysteresis as depicted in Fig. 10. In addition, any specimen which is cooled to 50 K and then warmed to 77 K will exhibit jumps when cooled again; further cyclings do not alter the results. Such resistive changes would require that the radius decrease by about 3% and that the specimen adhere strongly to the glass on successive cyclings. This indicates that the jumps are not associated with the 82 K transition and that they are not due to sudden thermal contractions. In any event, these mechanisms do not explain the resistivity minimum seen upon warming. It is quite possible that the minimum indicates a transition to a new state whose nature is undetermined but which may be magnetic (*34*).

Below the resistance minimum, the resitivity decreases smoothly with no discontinuities. The Bloch-Grüneisen resistivity, normalized to the measured resistivity at 55 K and using $\theta_R = 55$ K, is shown as the solid curve in Fig. 8. The Bloch-Grüneisen resistivity is clearly a poor fit to the experimental data. However this is not too surprising. Umklapp scattering, which is ignored in the derivation of the Bloch-Grüneisen relationship, is known to contribute substantially to both the high and low-temperature resistivity in other metals.

B. Low-Temperature Magnetoresistance

The magnetoresistance results are shown in Fig. 11. The value of the resistivity at 4.2 K in zero field, as measured in a glass dewar system, is 0.15 $\mu\Omega$-cm. The resistivity at 1.66 K was not measured in this run but based upon previous measurements it is estimated to be 0.08 $\mu\Omega$-cm.

The results for both runs are similar. They can each be represented fairly accurately at low fields by about a 1.5 power law, that is, $\rho(B) \propto B^{1.5}$. At high fields the exponent is 0.6 at 1.66 K and 0.9 at 4.2 K. Regardless of the 1.66 K resistivity one chooses to use, the data from both runs do not fall on the same curve; that is, Kohler's rule

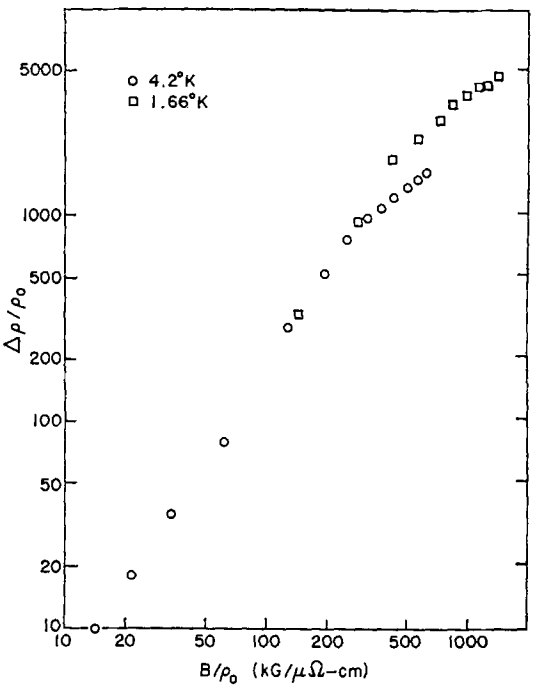

FIG. 11. Magnetoresistance of lithium tetraammine at 4.2 K and 1.66 K.

is not obeyed. In light of results on many other metals, this is not at all surprising.

Lithium tetraammine is an unusual metal. It is one of only three monovalent hcp metals; the others being the low-temperature phases of lithium and sodium. Though no conclusive data are available the following arguments indicate that for these metals one would not expect compensation despite the fact that sZ is even (see Section II) (*38*).

In the absence of any spin-orbit coupling, the first Brillouin zone of an hcp metal has no band-gap across the hexagonal faces (see Fig. 1). If there were a band-gap, one would reassemble the caps of the sphere from the second zone into the first zone to form lens-like electron pockets (see Fig. 1d). This leaves in the first zone a piece of an extended, undulating cylinder also shown in Fig. 1d. Both surfaces are electron sheets and therefore the metal is uncompensated [both F and J are zero, see Eq. (1)]. This Fermi surface then consists of a cylinder which gives open orbits along the c-axis and a lens which gives only closed orbits in the absence of magnetic breakdown (*14*).

In the absence of spin-orbit splitting, or in magnetic fields sufficiently large to cause magnetic breakdown across the hexagonal faces,

the topologically correct Fermi surface is obtained by combining the first and second bands into a single surface within a double zone as shown in Fig. 1c (*14*). In this case, the free electron Fermi sphere is centered at Γ. For a monovalent metal, the Fermi surface is a sphere. Hence, there are no open orbits.

The proximity of the free electron sphere to the nearest zone face depends on the c/a ratio. For $c/a = 1.43$, the sphere just contacts the Brillouin zone at point M (see Fig. 1b). For $Li(NH_3)_4$, $c/a = 1.58$. Therefore, the free electron sphere does not intersect the zone boundary. The actual Fermi surface depends on the band gap at point M. Since the free electron sphere is close to the BZ boundary, the real Fermi surface is likely to make contact in the vicinity of points M and form necks similar to those in copper (but probably of larger cross-sectional area). This might also be true at the top of the double zone.

Since the double zone has twice the volume of the single zone, it will be only half full. Thus one expects that hcp lithium, sodium and lithium tetraammine will be uncompensated metals. Looked at in the formulation summerized by Eq. (1), F and J are both zero and there are two electrons per unit cell. Because the low atomic number of lithium gives very small spin-orbit splitting across the hexagonal faces, the double zone is correct (magnetic breakdown in beryllium across these faces occurs at about 1 G). Thus, if the structure of lithium tetraammine below 77 K is hcp, it should be uncompensated. Note, however, that the resistance minimum near 70 K may well mark a transition in which the crystal structure changes again.

As seen in Fig. 11, the magnetoresistance of lithium tetraammine shows a marked decrease in slope at fields greater than about 50 kG. Except in the case of nickel, where the degree of compensation is affected by the magnetic ordering (*39*), no compensated polycrystalline metal has been observed to have a transverse magnetoresistance that increases less rapidly with increasing field. The arguments above, combined with both the tendency towards saturation and the low field slope of 1.5, indicate that lithium tetraammine is not a compensated metal. The large magnetoresistance could be due to the presence of a large number of open orbit carriers, indicating that the Fermi surface contacts the Brillouin zone over a wide area.

In light of this discussion, it is possible to make some remarks that bear on the observed T^2 term in the resistivity (*8*, *41*). In particular, if the metal is not compensated the electron density may be calculated from the atomic density. In this case, the Fermi degeneracy temperature, T_F, is that appropriate for a Fermi energy of about 1 eV, namely $T_F \simeq 11{,}000$ K. Therefore, resistive mechanisms which rely on the second term in the expansion of the Fermi function will have exceedingly small coefficients at the temperatures involved here (*40*). The large T^2 term found in some transition metals has been ascribed to electron–electron scattering with a rate enhanced by the large density of states at the Fermi surface of transition metals (*42*). This is corroborated by the large electronic specific heat found in these metals (*43*). Unfortunately, the specific heat of the lithium tetraammine system has not been measured at temperatures sufficiently low to permit the electronic component to be isolated. There are no other measurements which enable one to estimate the importance of the electron–electron scattering.

A mechanism that has been suggested for the T^2 term in the resistivity of ytterbium is scattering from spin wave fluctuations arising near a transformation to an exitonic state (*44*). This mechanism, however, also postulates a two-band model. From our previous discussion, this appears to be unlikely.

Umklapp scattering can also contribute a T^2 term to the resistivity (*45*). However, this will not occur over a very wide temperature range and the persistence of the T^2 term to 2 K argues against this hypothesis (*8*, *41*). It seems that the most likely mechanism for the T^2 term, if it can be attributed to a single mechanism, will be scattering from spin fluctuations or other magnetic instabilities.

V. Conclusions

General theoretical arguments concerning the expected Fermi surface for monovalent hcp metals and the experimental evidence of a tendency towards saturation of the magnetoresistance at high fields indicate that lithium tetraammine is not a compensated metal. The resistivity minimum near 70 K may be associated with a phase transition in either the electronic or crystal structure. Before any more definitive conclusions can be drawn, the structure and other physical properties of the material must be determined down to quite low temperatures. Of particular

interest would be the electronic specific heat, explication of the phase diagram, X-ray or neutron diffraction studies at liquid helium temperatures, and the numerous experiments which would become possible if suitable single crystals could be prepared.

VI. Acknowledgments

We are grateful to Al Garroway for his collaboration in the specimen preparation and the construction of the vacuum line and to D. K. Wagner for many helpful and stimulating discussions relating to transport theory.

References

1. N. W. Ashcroft and G. Russakoff, *Phys. Rev.* **1**, 39 (1970).
2. M. J. Sienko and P. Chieux, "Metal Ammonia Solutions" (J. J. Lagowski and M. J. Sienko, Eds.), p. 350, Butterworth, London (1969).
3. J. A. Vanderhoff and J. C. Thompson, *J. Chem. Phys.* **55**, 105 (1971).
4. D. E. Bowen, *J. Chem. Phys.* **51**, 1115 (1969).
5. H. Jaffe, *Z. Physik* **93**, 751 (1935).
6. N. Mammano and L. V. Coulter, *J. Chem. Phys.* **50**, 393 (1969).
7. J. A. Morgan and J. C. Thompson, *J. Chem. Phys.* **47**, 4607 (1967).
8. R. C. Cate and J. C. Thompson, *J. Phys. Chem. Solids* **32**, 443 (1971).
9. J. A. Morgan, R. L. Schroeder, and J. C. Thompson, *J. Chem. Phys.* **43**, 4494 (1965).
10. W. J. McDonald and J. C. Thompson, *Phys. Rev.* **150**, 602 (1966).
11. E. W. LeMaster and J. C. Thompson, *J. Solid State Chem.* **4**, 163 (1972).
12. N. Mammano and M. J. Sienko, *J. Amer. Chem. Soc.* **90**, 6322 (1968).
13. E. Fawcett, *Adv. Phys.* **13**, 139 (1964).
14. L. M. Falicov and Morrel H. Cohen, *Phys. Rev.* **130**, 92 (1963).
15. W. Harrison, *Phys. Rev.* **118**, 1182 (1960).
16. I. M. Lifshitz, M. IA. Azbel', and M. I. Kaganov, *JETP* **4**, 41 (1957).
17. J. L. Olsen, "Electron Transport in Metals," p. 68, Interscience, New York (1962).
18. Purchased from Alfa Inorganics, Beverley, Massachusetts.
19. P. Chieux, Ph.D. Thesis, Cornell University (1970).
20. T. Warshawsky, *J. Catal.* **3**, 291 (1964).
21. D. R. Clutter and T. J. Swift, *J. Amer. Chem. Soc.* **90**, 601 (1968).
22. I. Warshawsky, *J. Inorg. Nucl. Chem.* **22**, 601 (1963). Care was taken in the specimen preparation to avoid contamination which would tend to promote the decomposition of the lithium ammonia solutions. Thus great effort was invested in purifying the ammonia, cleaning the glass walls, and handling the lithium. However, it was felt that purification of the lithium itself would not be worthwhile since the dominant impurities in the lithium are other alkali metals. Li–NH_3 specimens prepared for NMR measurements with the same apparatus showed a typical degradation of less than 0.5% of the original Li charge. These were specimens about 8 months old and with a considerable history at elevated temperatures. Since degradation of this order could not be prevented, the effort of purifying further the 99.9% lithium was not warranted.
23. Purchased from Matheson Company, Inc., East Rutherford, New Jersey.
24. Richard A. Ogg, Jr., *J. Chem. Phys.* **22**, 560 (1954).
25. Gilbert W. Castellan, "Physical Chemistry," p. 43, Addison Wesley, Reading, Massachusetts (1964).
26. "American Institute of Physics Handbook" (Dwight E. Gray, coordinating editor), 2nd Edition, McGraw-Hill, New York, (1963).
27. Dow-Corning #705.
28. NBS traceable Class M weight (maximum tolerance of 5.4 μg), purchased from Cahn Instruments, Paramount, California.
29. M. D. Rosenthal and B. W. Maxfield, to be published.
30. J. E. Zimmermann, *Rev. Sci. Inst.* **32**, 402 (1961).
31. J. W. Ekin and D. K. Wagner, *Rev. Sci. Inst.* **41**, 1109 (1970).
32. N. F. Mott, *Proc. Roy. Soc.* (*London*) **146**, 465 (1934).
33. G. J. Meaden, "Electrical Resistance of Metals," p. 34, Plenum Press, New York (1965).
34. W. S. Glaunsinger, S. Zolotov, and M. J. Sienko, to be published.
35. J. S. Dugdale and D. Gugan, *Cryogenics* **2**, 103 (1961).
36. F. M. Kelly and D. K. C. MacDonald, *Can. J. Phys.* **31**, 147 (1953).
37. S. Zolotov and M. J. Sienko, to be published.
38. D. Gugan and B. K. Jones, *Helv. Phys. Acta*, **36**, 7 (1963). From those magnetoresistance measurements on multiphase, polycrystalline lithium, they conclude that only closed orbits exist in the hexagonal phase. This indicates that the double zone is correct, as the long undulating cylinder in Fig. 1d cannot then exist.
39. E. Fawcett and W. A. Reed, *Phys. Rev.* **131**, 2463 (1963).
40. A. H. Wilson, "The Theory of Metals," pp. 13, 227, University Press, Cambridge (1965). If the Fermi surface consists of several pieces, each will have a different degeneracy temperature. For instance, the degeneracy temperature of the lens in Fig. 1d will be lower than that of the second piece. However, even

if the single zone is correct, the degeneracy temperature of the lens in $Li(NH_3)_4$ will be the order of 3000 K and second order terms will be negligible.

41. M. D. ROSENTHAL AND B. W. MAXFIELD, to be published.

42. G. K. WHITE AND S. B. WOODS, *Phil. Trans. Roy. Soc. (London)* **A251**, 273 (1959).

43. See C. KITTEL, "Introduction to Solid State Physics," 4th Editon, p. 254, John Wiley and Sons, New York (1971).

44. D. JEROME, M. RIÈUX, J. FRIEDEL, *Phil. Mag.* **23**, 1061 (1971).

45. J. W. EKIN, private communication and also Walter E. Lawrence, Ph.D. Thesis, Cornell University (1970).